Homopolycyclotrimerization of A_4-Type Tetrayne: A New Approach for the Creation of a Soluble Hyperbranched Poly(tetraphenylethene) with Multifunctionalities

Rongrong Hu,[1,2] Jacky W. Y. Lam,[1,2] Min Li,[2] Haiqin Deng,[2] Jie Li,[2] Ben Zhong Tang[1,2,3]

[1]The Hong Kong University of Science & Technology (HKUST) Shenzhen Research Institute, No. 9 Yuexing 1st RD, South Area, Hi-Tech Park, Nanshan, Shenzhen, China, 518057
[2]Department of Chemistry, Institute of Molecular Functional Materials and Division of Biomedical Engineering, HKUST, Clear Water Bay, Kowloon, Hong Kong
[3]Guangdong Innovative Research Team, SCUT-HKUST Joint Research Laboratory, State Key Laboratory of Luminescent Materials and Devices, South China University of Technology (SCUT), Guangzhou, 51064, China
Correspondence to: B. Z. Tang (E-mail: tangbenz@ust.hk)

Received 29 June 2013; accepted 1 August 2013; published online 26 August 2013
DOI: 10.1002/pola.26897

ABSTRACT: A tetraphenylethene-containing A_4-type tetrayne, named 1,1,2,2-tetrakis(4-ethynylphenyl)ethene is synthesized and its $TaCl_5$-Ph_4Sn catalyzed homopolycyclotrimerization affords hyperbranched poly(tetraphenylethene) with high molecular weight ($M_w = 280{,}000$) in high yield (97%). The polymer shows good solubility and high thermal stability. It is aggregation-enhanced emission (AEE)-active and functions as a fluorescent chemosensor for explosive detection with a superamplification effect and large quenching constants up to 758,000 M^{-1}. The polymer shows high and tunable refractive indices (RI = 1.9288−1.6746) in a wide wavelength region. Porous fluorescent polymer thin film is prepared by breath figure (BF) methods and real-time monitoring of the elusive BF formation process is realized. Photolithography of the thin films readily generates well-resolved fluorescent photopattern without and with porous secondary structure. The polymer is metallified and pyrolysed to give magnetic ceramics with high magnetic susceptibilities ($M_s = 83$ emu/g) and near-zero coercivity ($H_c = 0.08$ kOe). © 2013 Wiley Periodicals, Inc. J. Polym. Sci., Part A: Polym. Chem. **2013**, *51*, 4752–4764

KEYWORDS: conjugated polymers; hyperbranched; luminescence; porous materials; structure-property relationships

INTRODUCTION Hyperbranched polymers possess superior properties than their linear counterparts and have attracted much attention among polymer scientists for their globular architectures and numerous functional end groups on the periphery.[1] Compared with their dendritic congeners whose perfect structures are prepared from elaborate multistep methods and painful isolations, hyperbranched polymers exhibit similar properties, but they can be easily accessed from simple single-step polymerizations.[2] Among various methods, polycondensations of AB_2- or $(A_2 + B_3)$-type monomers are widely used for the preparations of hyperbranched polymers.[3] However, AB_2-type monomers with two mutually reactive functional groups in one molecule lead to self-reaction during preparation and storage. On the other hand, in the $A_2 + B_3$ monomer strategy, strict stoichiometric balance between the two monomers is required in order to achieve high molecular weight polymers. A_2-type monomers hence show great advantages in the preparation of hyperbranched polymers through polymerization approaches such as ring-opening polymerization and self-condensing vinyl polymerization.[4] In particular, A_2-type diyne monomers are stable at room temperature and their polycyclotrimerizations can proceed smoothly under control, thus providing an efficient method to prepare functional hyperbranched conjugated polymers with high molecular weights in high yields. Using such synthetic tool, a large variety of functional hyperbranched polyphenylenes with unique properties such as high thermal stability, photocurability, efficient light emission and large optical nonlinearity were successfully synthesized.[5] Through copolycyclotrimerizations of aryldiynes with aromatic or aliphatic monoynes, the resulting polymers possess improved solubility and properties, though their structures become complicated.[6]

A_3- or A_4-type monomers, on the other hand, usually serve as crosslinking units in the copolymerizations with AB-type

Additional Supporting Information may be found in the online version of this article.

monomers to form 3 or 4-arm star-shaped polymers and are used in very low concentrations.[7] Homopolymerizations of A_n-type ($n \geq 3$) monomers, especially those ones contain aromatic rings are rarely reported[8] as the polymerizations easily run out of control and generate insoluble crosslinked gels. The intractability renders the polymers less useful from the viewpoint of practical scope. Direct utilization of A_3- or A_4-type monomers for polymer synthesis remains to be a big challenge. If processable polymers can be obtained from homopolymerizations of A_3- or A_4-type monomers, polymers with more terminal groups, more branching sites and superior properties than polymers obtained from A_2-type monomers can be expected.

Recently, we observed a phenomenon of "aggregation-induced emission (AIE)" in a series of propeller-like compounds such as tetraphenylethenes (TPE) and siloles.[9] The compounds were found to be virtually non-luminescent in solutions but became highly emissive when aggregated as nanoparticles in poor solvent or in the solid states. AIE phenomenon is exactly opposite to the thorny aggregation-caused quenching effect observed in many conventional luminophors. It enables the AIE luminogens to find an array of practical applications, taking advantage of their high solid-state fluorescence efficiency. Almost all the AIE compounds possess a nonplannar conformation due to the steric hindrance between the periphery aryl rings. Thus, polymers prepared from AIE monomers are expected to show large interchain distances and hence weak intermolecular interactions. Large free volume is generated in the polymers to accommodate more solvent molecules, which can facilitate the dissolution process. Indeed, soluble hyperbranched polymer *hb*−P**2** was successfully obtained by homopolymerization of A_2-type TPE-containing diyne monomer **2** in high molecular weight of 160,000 in nearly quantitative yield [Scheme 1(A)].[10] Compared with polymers obtained from A_2-type monomers, those prepared from A_4-type monomers are more desirable because they possess higher interior density of functional units, more branching sites and functional end groups. However, such possibility has seldom been explored, mainly due to the concern of crosslinking reaction and solubility of the resulting polymers.

In this work, we take the challenge to explore the utility of A_4-type monomers for constructing processable polymers. A TPE-containing tetrayne, named 1,1,2,2-tetrakis(4-ethynylphenyl)ethene (**1**) was prepared and successfully transformed into soluble hyperbranched polymer *hb*−P**1** by alkyne polycyclotrimerization [Scheme 1(B)]. *hb*−P**1** possesses a three dimensional topological structure and shows extended electronic conjugation. Despite of its high molecular weight, it dissolves readily in organic solvents and exhibits good film-forming ability, thanks to the twisted conformation of the TPE units. It also enjoys high thermal stability and features with aggregation-enhanced emission (AEE) characteristic. Both uniform and porous fluorescent films of *hb*−P**1** can be easily obtained by spin-coating and breath figure (BF) approaches, respectively. It is worth mentioning that the real-time monitoring of the long-unknown BF formation process is realized through observation under the fluorescence microscope, taking advantage of the AEE feature of *hb*−P**1**. Other high-tech applications of **1** and *hb*−P**1** such as mechanochromic materials, fluorescent chemosensor for explosive detection, photoresist materials, materials with modulable refractivity and magnetic ceramics are also explored and presented.

EXPERIMENTAL

Materials

THF and toluene were distilled under normal pressure from sodium benzophenone ketyl under argon immediately prior to use. Tantalum(V) chloride ($TaCl_5$), tetraphenyltin (Ph_4Sn), and 1,2-dichloroethane were all purchased from Aldrich and used as received without further purification. Octacarbonyldicobalt $Co_2(CO)_8$ was purchased from Fluka and stored in a refrigerator. Monomer **1** was prepared according to the reported procedures.[11]

Instrumentation

IR spectra were recorded on a Perkin-Elmer 16 PC FT-IR spectrophotometer. ^{1}H NMR spectra were measured on Bruker ARX 300 or 400 NMR spectrometers using dichloromethane-d_2 as solvents and tetramethylsilane (TMS; $\delta = 0$ ppm) as internal standard. Number-(M_n) and weight-average (M_w) molecular weights and polydispersity indices (PDI or M_w/M_n) of the polymers were estimated by gel permeation chromatography (GPC) using a Waters Associates liquid chromatograph equipped with a Waters 515 HPLC pump, a set of Styragel columns (HT3, HT4, and HT6; molecular weight range 10^2-10^7), a column temperature controller, a Waters 486 wavelength-tunable UV-Vis detector, a Waters 2414 differential refractometer, and a Waters 2475 fluorescence detector. The polymers were dissolved in THF (~2 mg/mL) and filtered through 0.45 μm PTFE syringe-type filters before being injected into the GPC system. THF was used as eluent at a flow rate of 1.0 mL/min. The column temperature was maintained at 40 °C, and the working wavelength of the UV-Vis detector was set at 254 nm. A set of monodisperse polystyrene standards (Waters) covering the molecular weight range of 10^3-10^7 were used for the molecular weight calibration. Thermogravimetric analysis (TGA) measurements were carried out under nitrogen or in air on a Perkin-Elmer TGA 7 analyzer at a heating rate of 10 °C/min. UV-Vis absorption spectra were measured on a Milton Roy Spectronic 3000 array spectrophotometer. Photoluminescence (PL) spectra were recorded on a Perkin-Elmer LS 55 spectrofluorometer. The X-ray photoelectron spectroscopy (XPS) experiments were conducted on a PHI 5600 spectrometer (Physical Electronics), and the core level spectra were measured using a monochromatic Al-K_α X-ray source ($h\nu = 1486.6$ eV). The analyzer was operated at 23.5 eV pass energy and the analyzed area was 800 μm in diameter. The structures of the ceramics were investigated by high-resolution transmission electron microscopy JEOL 2010F TEM. The X-ray diffraction (XRD) diagrams were recorded on a Philips PW 1830 powder diffractometer using

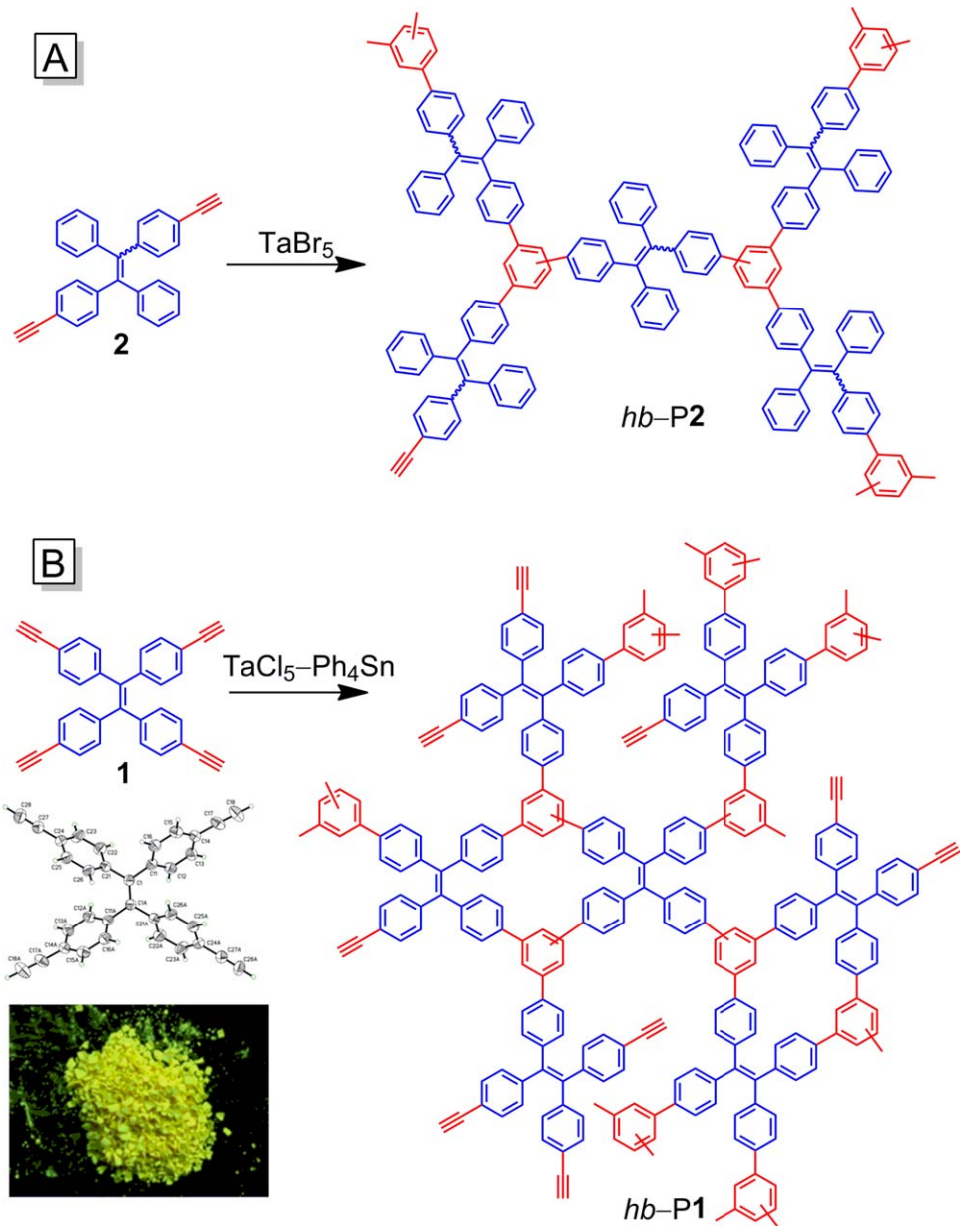

SCHEME 1 Synthesis of hyperbranched poly(tetraphenylethene)s by homopolycyclotrimerization of (A) A_2-type diyne and (B) A_4-type tetrayne. Inset: single crystal of **1** and the fluorescent image of *hb*−P**1**. [Color figure can be viewed in the online issue, which is available at wileyonlinelibrary.com.]

the monochromatized X-ray beam from a nickel-filtered radiation ($\lambda = 1.5406$ Å). Magnetization curves were recorded on a Lake Shore 7037/9509-P vibrating sample magnetometer (VSM) at room temperature. Refractive indices were determined on a JA Woolam Variable Angle Ellipsometry System with a wavelength tunable from 300 to 1000 nm. Time-resolved PL measurements were carried out on a Hamamatsu model C4334 streak camera coupled to a spectrometer, with a time resolution of 20 ps. The PL signals were collected at the emission peaks and the laser energy level for excitation was 4.8 mW. Decay in the PL intensity (I) with time (t) was fitted by a single-exponential function $y = A_1 \times \exp(-x/t_1) + y_0$ or double-exponential function $y = A_1 \times \exp(-x/t_1) + A_2 \times \exp(-x/t_2) + y_0$. Photo-oxidation reactions of the polymer films were conducted in air at room temperature using 365 nm light obtained from a Spectroline ENF-280C/F UV lamp at a distance of 5 cm from light source. The fluorescent photos were taken on an optical microscopy (Nikon ECLIPSE 80i) under UV light or blue light source.

RESULTS AND DISCUSSION

Polycyclotrimerization

The TPE-containing A_4-type tetrayne **1** was obtained according to our previous published article.[11] Its structure was confirmed by IR, NMR, and mass spectroscopies as

TABLE 1 Polymerization of 1[a]

Entry	[**1**] (M)	[cat]/[**1**] (%)	Time	Yield (%)	M_w[b]	PDI[b]	*S*
1	0.05	10	6 min	99	Gel		×
2	0.05	5	8 h	97	280,000	3.8	√
3	0.04	5	20 h	34	48,000	2.7	√
4	0.02	10	20 h	99	42,000	2.5	√
5	0.02	5	20 h	24	6,800	1.5	√

[a] Carried in toluene under nitrogen in the presence of $TaCl_5$-Ph_4Sn.
[b] Determined by GPC on the basis of a polystyrene calibration.
PDI = polydispersity index = M_w/M_n, *S* = solubility tested in common organic solvents such as THF, chloroform, and toluene: × = insoluble and √ = soluble.

well as single crystal X-ray diffraction (Scheme 1). Its polycyclotrimerization was catalyzed by $TaCl_5/SnPh_4$ cocatalyst.[12] To obtain soluble hyperbranched polymer with high molecular weight, the reaction conditions for the polymerization is optimized. The homopolymerization was first tested in a relatively low monomer concentration of 0.05 M. After reaction for 6 min at room temperature, an insoluble gel was formed quantitatively (Table 1; no. 1). Delightfully, when the catalyst loading was decreased by half, while keeping the monomer concentration constant, a soluble hyperbranched polymer with high M_w of 280,000 was obtained in 97% yield after 8 h (Table 1; no. 2). Processable polymers are also obtained in dilute monomer solution with constant amount of catalyst but their molecular weight becomes lower. The polymerization performed at both low monomer and catalyst concentrations generate only polymers with low molecular weight in low yield even after a long reaction time (Table 1; no. 5). Evidently, to suppress undesirable crosslinking reaction while preserving promising polymerization result, it is more effective to precisely control the catalyst concentration.

Structure Characterization

Both **1** and *hb*−P**1** were thoroughly purified and fully characterized by standard spectroscopic methods, from which satisfactory analysis data corresponding to their expected structures were obtained (see Supporting Information for details). For example, the strong absorption band at 3270 cm^{-1} in the IR spectrum of **1** is associated with its ≡C−H stretching vibration, while the peak at 2107 cm^{-1} is related to C≡C stretching vibration (Supporting Information Fig. S1). These two bands are still observed in the spectrum of *hb*−P**1**, at slightly higher wavenumbers (3294 and 2109 cm^{-1}) but with much lower intensity, indicating that most of the triple bonds of **1** have been consumed by the polymerization and the remaining triple bonds exist as end groups on the periphery of the polymer. Meanwhile, the absorption bands at 3031 cm^{-1} and 1600 cm^{-1} originated from Ar−H stretching vibration and aromatic C=C skeleton vibration are broadened after the polymerization due to the formation of new benzene rings.

Analysis by ^{1}H NMR spectroscopy gives similar results. The acetylene proton of **1** resonates at δ3.13, which becomes weaker and broader in the spectrum of *hb*−P**1** (Supporting Information Fig. S2). The integral of the acetylene proton peak of *hb*−P**1** is larger than that of *hb*−P**2**, indicating more terminal groups in *hb*−P**1** than in *hb*−P**2**.[10] The aromatic proton absorptions of **1** exist as two doublets at δ7.26 and 6.99, which transform into broad multiplets after polymerization due to the formation of new 1,3,5- and 1,2,4-trisubstituted benzene rings in the polymer. The polymer backbone was constructed from conjugated benzene rings and it was hard to differentiate terminal, linear and dendritic units through NMR analysis. The important parameter, the degree of branching of such a complicated A_4-type polymerization system is thus difficult to estimate. From the ^{1}H NMR spectra, the ratio of terminal acetylene protons and aromatic protons is 0.13/1. It is thus calculated that about 57.5% of the acetylene groups in the monomer still remain as terminal groups and the relatively high ratio indicate that crosslinking between polymer branches is less favored.

Solubility and Thermal Stability

Though *hb*−P**1** are mainly constructed from aromatic rings, it is readily soluble in common organic solvents such as toluene, dichloromethane, chloroform, THF, and so forth, and possesses good film-forming property. Tough thin film can be easily obtained by simple spin coating method and it is stable under ambient condition for several months. The thermal stability of *hb*−P**1** was evaluated by thermogravimetric analysis (TGA). As shown in Supporting Information Figure S3, *hb*−P**1** exhibits outstanding thermal stability, exhibiting 5% weight loss at temperature (T_d) as high as 525 °C under nitrogen and 461 °C in air. Such values are much higher than *hb*−P**2** (462 °C under nitrogen and 417 °C in air). It is noteworthy that about 60% of its weight is still retained even when heated to 800 °C under nitrogen, which is rarely observed in pure organic materials and suggesting that *hb*−P**1** is a promising precursor to ceramic materials. The high thermal stability of *hb*−P**1** may be mainly associated with the acetylene polymerization of its periphery alkyne groups, which further crosslinks the polymer and hence imparts it with higher resistance towards thermolysis.

Photophysical Properties

The UV spectrum of **1** in dilute THF solution exhibits an absorption maximum at 341 nm with a strong peak at 274 nm (Supporting Information Fig. S4). Polymer *hb*−P**1** absorbs at 347 nm, suggesting that it possesses an enhanced electronic conjugation due to the electronic communication between the TPE units and the newly formed benzene rings. The spectral pattern alters little when *hb*−P**1** is fabricated into thin film in the solid state, thanks to the weak interstrand interaction caused by the propeller-like TPE units.

The dilute THF solution of **1** shows no emission under UV illumination [Supporting Information Fig. S5(A)]. When a large amount of water (≥85%) was added to the THF solution, the solution becomes emissive. The higher the water content, the stronger the light emission. Since **1** is not soluble in water, its molecules must have been aggregated in

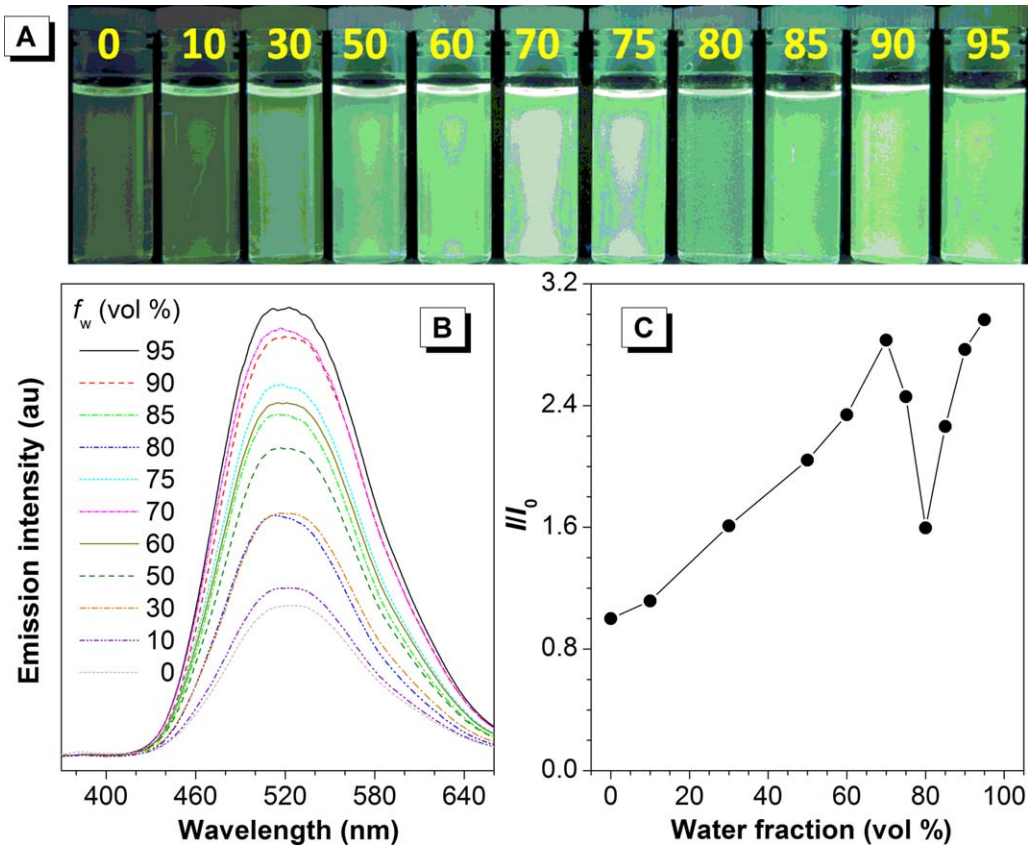

FIGURE 1 (A) Photographs of *hb*−P**1** in THF/water mixtures with different water fractions (f_w) taken under UV illumination. (B) Emission spectra of *hb*−P**1** in THF/water mixtures with different water fractions (f_w). (C) Plot of relative PL intensity (I/I_0) versus the composition of the aqueous mixtures of *hb*−P**1**. Solution concentration: 10 μM; excitation wavelength: 346 nm. [Color figure can be viewed in the online issue, which is available at wileyonlinelibrary.com.]

aqueous mixtures with high water contents. Clearly, **1** is a typical AIE compound. Unlike **1**, *hb*−P**1** is somewhat emissive in THF solution [Fig. 1(A)], presumably due to the partially fixed intramolecular rotations by the polymer skeleton. The fluorescence is enhanced when the polymer aggregates in the presence of water, displaying a phenomenon of aggregation-enhanced emission characteristic. The emission intensity is slightly weakened at 80% water content. The exact reason for this remains unclear at present but may be related to the poor stability of such aqueous suspension. Visible precipitates can be observed from naked eyes which has lowered the effective concentration of the aqueous mixture and hence the light emission.

In addition to direct impression by visual observation, the emission behaviors of **1** and *hb*−P**1** in solution and aggregated states were studied by a photoluminescence (PL) spectrometer. Compound **1** is practically nonemissive in THF and the PL spectrum is basically a flat line parallel to the abscissa. When 80% of water is added to the THF solution, an emission peak emerges at 510 nm, whose intensity is enhanced progressively with increasing water content. At 95% aqueous mixture, the PL intensity is 238-fold higher than that in THF solution [Supporting Information Fig. S5(B,C)]. Despite weak, *hb*−P**1** emits at 523 nm in THF solution. The emission intensity starts to increase even in the presence of a small amount of water and reaches its maximum value at 95% water content [Fig. 1(B,C)]. We have proposed that restriction of intramolecular rotation is the main cause for the AIE phenomenon. In THF solution as well as THF/water mixture with low water content, the molecules of **1** exist as isolated species and are free to rotate with little constraint. However, the TPE units in *hb*−P**1** are knitted together by benzene rings, which have partially restricted their intramolecular rotation and hence make the polymer emissive in the solution. Compared with **1**, *hb*−P**1** should be more ready to form aggregates in aqueous mixture owing to its higher hydrophobicity and poorer solubility, thus making its PL process more sensitive to the change in the surrounding solvent medium. It is noteworthy that both aqueous mixtures for **1** and *hb*−P**1** are macroscopically homogeneous and visually transparent without precipitates even at high water content of 95%, suggesting that the aggregates are nanosized as proved by the analysis from transmission electron microscopy (Supporting Information Fig. S6).

To get insight into the photophysical properties of **1** and *hb*−P**1**, the PL decay dynamics were studied by time-resolved fluorescence spectrometer (Supporting Information Fig. S7 and Table S1). In the aggregated state, the excited

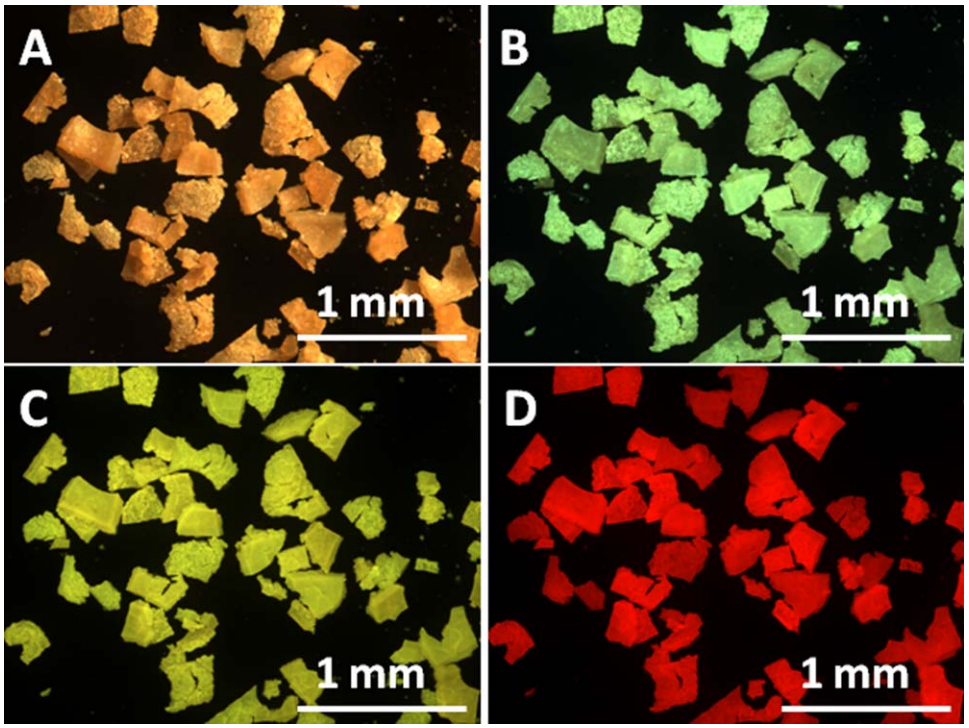

FIGURE 2 Fluorescent images of *hb*−P**1** powder taken under different light illuminations. Excitation wavelength: (A) daylight, (B) 330−380 nm, (C) 450−490 nm and (D) 510−550 nm. [Color figure can be viewed in the online issue, which is available at wileyonlinelibrary.com.]

states of **1** relax in a single-exponential fashion with lifetime of 0.54 ns. In the solid state, the relaxation becomes slower and the decay curve is better fitted by a double-exponential function with a mean lifetime of 1.84 ns, indicating that two relaxation pathways are involved in the decay process. A similar trend was observed for *hb*−P**1** with mean lifetime of 0.24, 0.48 and 0.74 ns, being detected in the solution, aggregated and solid states, respectively.

The PL spectrum of *hb*−P**1** in the aggregated state is broad because of the presence of segments with various conjugation lengths or band gaps. Thus, when irradiated with different wavelengths, the polymer may show various emission colors. Indeed, the polymer powder appears yellow under daylight, which gives green, yellow and red emissions when exposed to UV, blue and green illuminations, respectively (Fig. 2).

Mechanochromism

Mechanochromic luminescent materials have attracted much attention in recent years because of their potential applications in camouflage and optical information storage systems.[13] With such regard, we tested whether the present material shows this property. UV irradiation of the solid powder of **1** induces a sky blue emission at 477 nm. Interestingly, after gentle grinding with a glass rod, the powder shows green emission, whose PL spectrum is 28 nm red-shifted from that of the untreated one (Fig. 3). Such color switching process is reversible and the PL spectrum is fully reinstalled when the ground sample is fumed with acetone vapor for 2 min due to the recrystallization of the molecules. It can be repeated many times without fatigue as these stimuli are nondestructive in nature. According to our previous investigation, the mechanochromic property of **1** should be originated from the morphological change from the thermodynamically stable crystalline phase to the metastable amorphous state.[14]

Explosive Detection

Sensors based on fluorescent conjugated polymers have attracted much interest due to their amplified response and superior sensitivity to analytes, in comparison to their low molar mass congeners.[15] Generally, intrinsic autoaggregation and analyte-induced aggregation of the conjugated polymers will cause fluorescence self-quenching effect, which greatly reduces the sensing performance.[16] However, aggregation is beneficial to the emission of AEE-active polymers. TPE-containing *hb*−P**1** is AEE–active and possesses a three-dimensional topological structure with abundant internal voids for capturing analyte species. It also has multi-dimensional excitonic migration pathways, which may lead to superior signal-amplifying effect and binding capability to analytes through Lewis acid-base interactions.[9,17] As such, we explored the utility of *hb*−P**1** as chemosensor for picric acid (PA) detection because of the involved antiterrorism implications.[18] The nanoaggregates of *hb*−P**1** in THF/water mixtures with 70 and 90% water contents are used as probes, for comparison, the detection was also performed in pure THF solution. With gradual addition of PA to the THF solution and aqueous nanoparticle suspensions of *hb*−P**1**, the emission is weakened progressively, while the PL

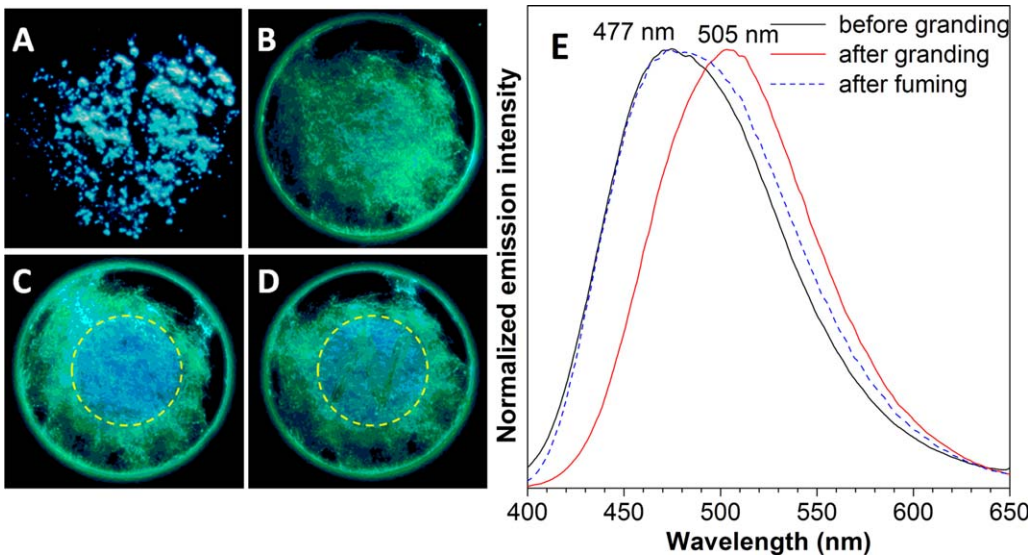

FIGURE 3 Fluorescent photographs of solid powder of **1** taken under 365 nm UV irradiation (A) before and (B) after grinding using a glass rod. The images in (C) and (D) are obtained by fuming the ground sample in (B) with acetone vapor and grinding a letter "N" in (C). (E) Change in the PL spectrum of solid powder of **1** by alternatively grinding and fuming processes. [Color figure can be viewed in the online issue, which is available at wileyonlinelibrary.com.]

spectral profile remains almost unchanged (Fig. 4). The PL quenching can be clearly seen at a PA concentration as low as 1 ppm. At a PA concentration of 1.26 mM, no PL signal is recorded from the THF solution. The emission from the polymer nanoaggregates is completely quenched at a much lower PA concentration down to 0.34 mM, suggesting that nanoaggregates show higher sensitivity for PA detection than their isolated species in THF solution. Due to the existence of numerous intermolecular cavities generated by the loose packing of the globular sphere of *hb*−P**1** containing bulky and twisted TPE units, the polymer nanoaggregates can interact with more PA molecules and hence exhibit higher sensing performance.

The Stern-Volmer plot of relative PL intensity (I_0/I) versus PA concentration shows upward-bending curves instead of linear lines [Fig. 4(D)], revealing that the fluorescence quenching becomes more efficient at higher quencher concentration. Such superamplification effect is associated with the AEE feature and hyperbranched structure of the polymer. Moreover, when more PA molecules are diffused into the internal cavities, the polymer swells. This imparts larger surface area, which can potentially interact with more analytes. On the other hand, the interior phenyl rings have relatively more space to rotate, which has quenched the light emission via nonradiative relaxation channel. Both effects result in higher sensitivity at high quencher concentration. In other words, the AIE/AEE-active conjugated hyperbranched polymers are anticipated to show superior sensory properties than that of other fluorescent polymers and are promising candidates for the development of fluorescent chemosensors and bioprobes with superamplified response and extremely low detection limit.

Compared with the AEE-active polymers in literatures with PL quenching constants of aggregate states ranging from 150,000 to 280,000 M^{-1},[19] *hb*−P**1** show three to fivefold higher sensitivity upon PA addition. In particular, large quenching constants up to 758,000 M^{-1} are deduced from the plot in 90% aqueous mixture of *hb*−P**1**, which are much higher than those of *hb*−P**2** (K_{sv} up to 429,000 M^{-1}), proving that hyperbranched polymer constructed from A_4-type monomer is a better fluorescent sensing material than that prepared from A_2-type monomer in the nanoaggregated states.

Light Refraction

The development of new processable organic materials with high and tunable refractive indices (RI or n) has became a fascinating and challenging field, owing to their potential applications in photonic and optoelectronic devices.[20] *hb*−P**1** possesses numerous aromatic rings and thus may show high RI value. Indeed, as shown in Supporting Information Figure S8, the thin film of *hb*−P**1** displays high RI values (1.9288−1.6746) in a wide wavelength region (400−1000 nm), which are larger than those of the commercially important optical plastics such as poly(methyl methacrylate) ($n \approx 1.49$), poly(ethylene terephthalate) ($n \approx 1.59$), as well as previously reported AEE-active polymers.[21] The RI values of *hb*−P**1** can be further tuned by UV irradiation. When the film was exposed to UV irradiation for 20 min, its RI values dropped to 1.6711−1.5862 in the same wavelength range, possibly due to the structural change in the polymer. The difference in the RI value (Δn) at 1000 nm after UV irradiation is as large as 0.1, demonstrating that the RI value of *hb*−P**1** can be facilely tuned by simple external stimulus, and thus enable it to find high-tech applications such as coating materials in advanced display systems.[22]

Microporous Film

Ordered microporous materials have been intensively investigated in the past decades for their potential application in diverse areas such as photonic/optoelectronic devices, catalysis, photonic crystals, separation membranes, biotechnology,

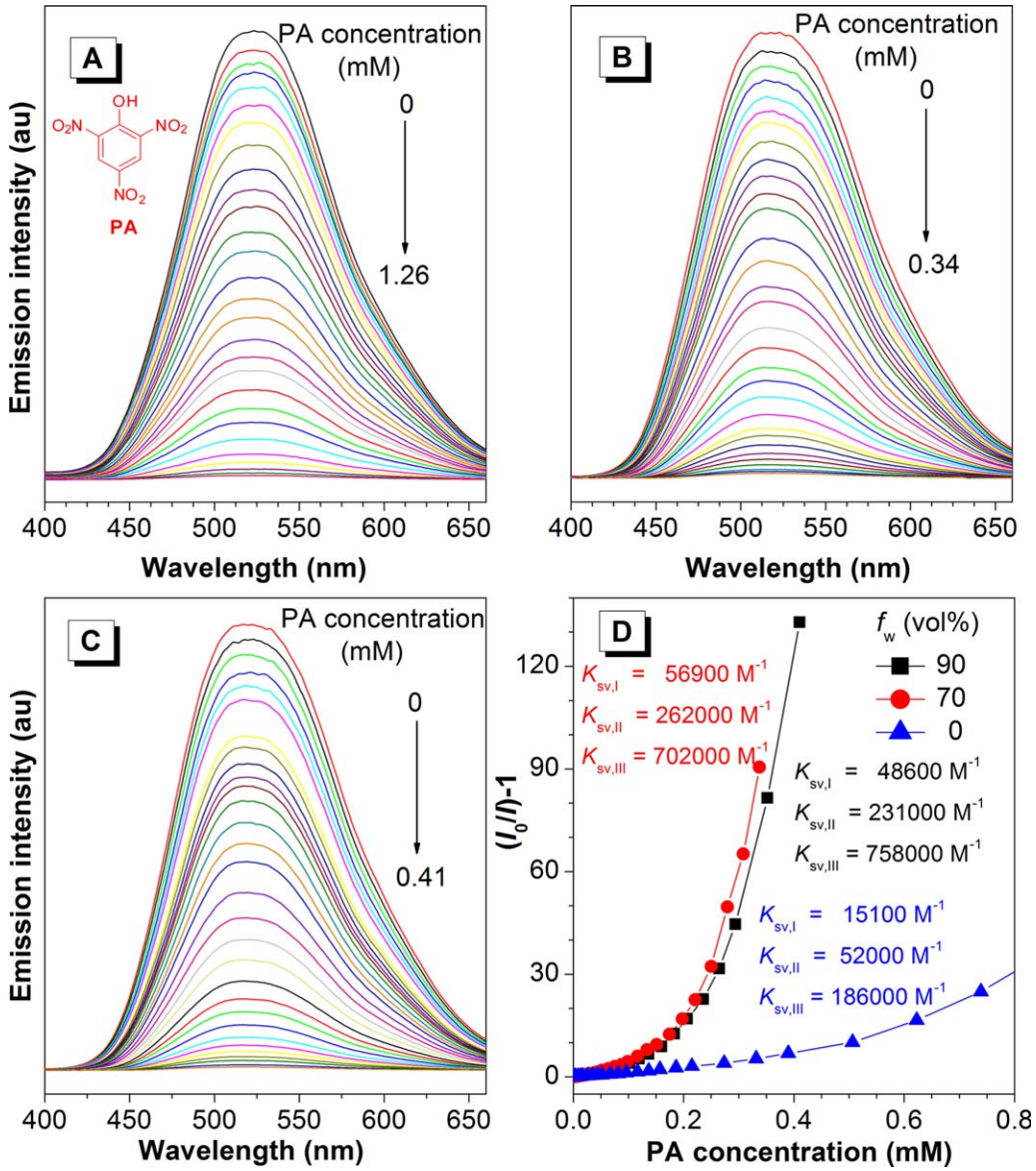

FIGURE 4 PL spectra of *hb*−P**1** in (A) THF solution, (B) 70% and (C) 90% aqueous mixtures with different PA concentrations. Concentration: 10 μM; excitation wavelength: 346 nm. (D) Stern-Volmer plots of $(I_0/I)-1$ values versus the PA concentrations in THF solution and THF/water mixtures with 70 and 90% water contents of *hb*−P**1**; I_0 = intensity at [PA] = 0 mM. [Color figure can be viewed in the online issue, which is available at wileyonlinelibrary.com.]

and so forth.[23] In particular, honeycomb-patterned films made by the self-assembly of small molecules and polymers have attracted increasing interest because of their fascinating morphology and potential applications.[24] The "bottom-up" breath figure (BF) method is the most popular approach to prepare ordered films from polymeric materials. It has attracted a high level of scientific and technological attention since the first report by Widawski et al. in 1994 due to its convenience, rapidity, economy and simplicity compared with other methods.[25] Hydrophobic, amphiphilic, linear, star-shaped and hyperbranched polymers, and even a few examples of small molecules have been used to fabricate honeycomb-patterned films. Typically, the honeycomb pattern is obtained by casting a polymer solution in a volatile solvent onto a substrate under humid condition. Water vapor condenses into water droplets at the surface of the polymer solution during solvent evaporation and then self-organizes into a well-ordered, hexagonal array that acts as a template directing the formation of film with an ordered microporous structure. The void diameter and spacing can be controlled by several factors including casting volume, concentration, polymer architecture and composition, humidity, air flow, temperature, additives, substrate pretreatment and so forth.[26] However, the exact BF formation mechanism is not fully understood due to the lack of direct experimental evidence.

The combination of accessible porosity with luminescence imparts materials with the capability of transducing the

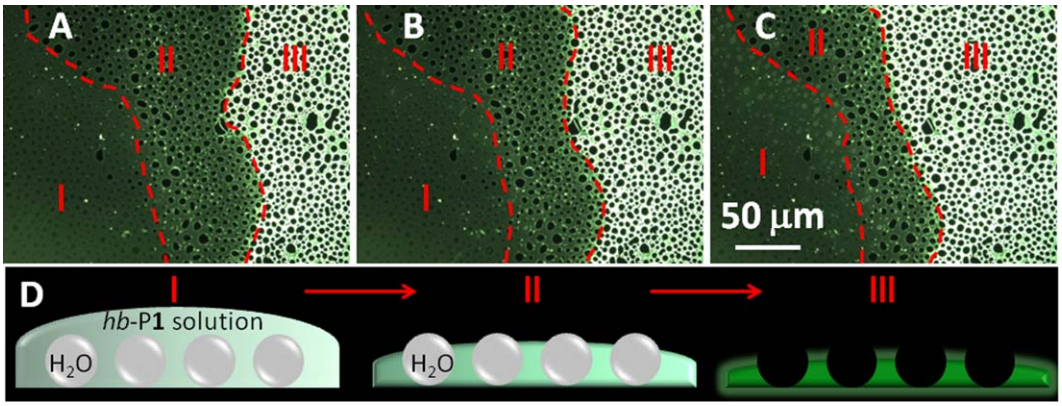

FIGURE 5 (A−C) Fluorescent images showing the formation of microporous film of *hb*−P**1** taken under UV light illumination. Excitation wavelength: 330−380 nm. (D) Schematic diagram of fluorescent microporous film formation process. [Color figure can be viewed in the online issue, which is available at wileyonlinelibrary.com.]

host-guest chemistry to detectable changes in their luminescence, thus generating guest-responsive multifunctional materials and making them promising candidates for chemical sensing applications.[27] However, such combination of stable porosity and intense fluorescence in materials is rarely reported. In order to fabricate luminescent honeycomb films, efforts have been made by mixing quantum dots[28] and fullerenes[29] with polymers. However, the dispersibility of fluorescent dye in polymer matrix is limited due to aggregation. To meet the challenge, conventional linear macromolecules were replaced by hyperbranched polymers to facilitate the dispersion, which has significantly enlarged the structural diversity and makes multifunctional self-assembly accessible.[30] We thus explore the utility of *hb*−P**1** to prepare fluorescent honeycomb-patterned films. Moreover, the AEE feature of *hb*−P**1** enables us to monitor the BF formation process through observation from the fluorescent microscopy image and video and hence elucidate the long-unknown mechanism of BF formation. To the best of our knowledge, this is the first direct experimental evidence of the BF formation process.

The fluorescent microporous film of *hb*−P**1** was prepared using the BF approach. Thanks to the AEE feature of *hb*−P**1**, the real-time BF formation process can be monitored with a fluorescent microscope as shown in the video provided in the Supporting Information. As demonstrated in Figure 5(A), during solvent evaporation, water condenses and buried by the polymer solution (phase I). When part of the solvent evaporates, the polymer solution becomes thinner, which exposes the underneath pores (phase II). After complete drying, fluorescent film with non-emissive pores is finally formed (phase III). Figure 5(A−C) clearly show that the solvent boundary line shifts from right to left, leaving a highly emissive microporous honeycomb film and providing an intuitive grasp of the mechanism for BF formation.

Figure 6(A−D) show the fluorescent honeycomb-patterned films fabricated from *hb*−P**1**. The pore size of the films is about a few micrometers. When excited by 330-380 nm light, they show intense green emission. When a longer excitation wavelength range of 450-490 nm is used, the emission color changes to yellow. The dye molecules tend to accumulate in the interface of water droplet and organic solvent during the evaporation process, as suggested by the stronger emission at the periphery of the pores. When all solvent and water are evaporated, an interesting repeatable phenomenon was observed: a small amount of yellow-emissive solid is found in the center of the green-emissive honeycomb film [Fig. 6(E,F)]. When observed under 450−490 nm blue light, the yellow-emissive portion can be clearly discerned from the green-emission portion. The reason for such phenomenon is still unknown at the present time but during BF formation, the polymer has segregated into two portions. The chains with higher molecular weight and longer conjugation length incline to separate from those with smaller number of repeating unit and lower conjugation due to the solubility difference.

Photopatterning

Since *hb*−P**1** has a broad emission color in the solid state and is photosensitive, it is thus potential fluorescent imaging and photoresist materials. A uniform and tough thin film of *hb*−P**1** was readily fabricated by spin-coating its 1,2-dichloroethane solution on solid support such as silicon wafer. When the film was UV-irradiated through a negative copper photomask, the color and emission of the exposed region faded and quenched, respectively. On the contrary, the covered square regions retained their original color and were still emissive. A two-dimensional fluorescent pattern with sharp edges was thus obtained, which showed green or yellow emission under UV or green light excitation, respectively [Fig. 7(A,B)]. The fluorescent patterns generated in air and under nitrogen are compared in Supporting Information Figure S9. The fluorescence fading is much faster in air than under nitrogen, indicating that oxygen plays a key role in the fluorescence quenching process or in other words, the PL annihilation is caused by photo-oxidation. Interestingly, *hb*−P**2** behaves differently toward UV irradiation.[10] Instead of photo-oxidation, the irradiated parts crosslink, become insoluble but are still emissive. The unexposed areas, however, retain soluble and can be removed by development in

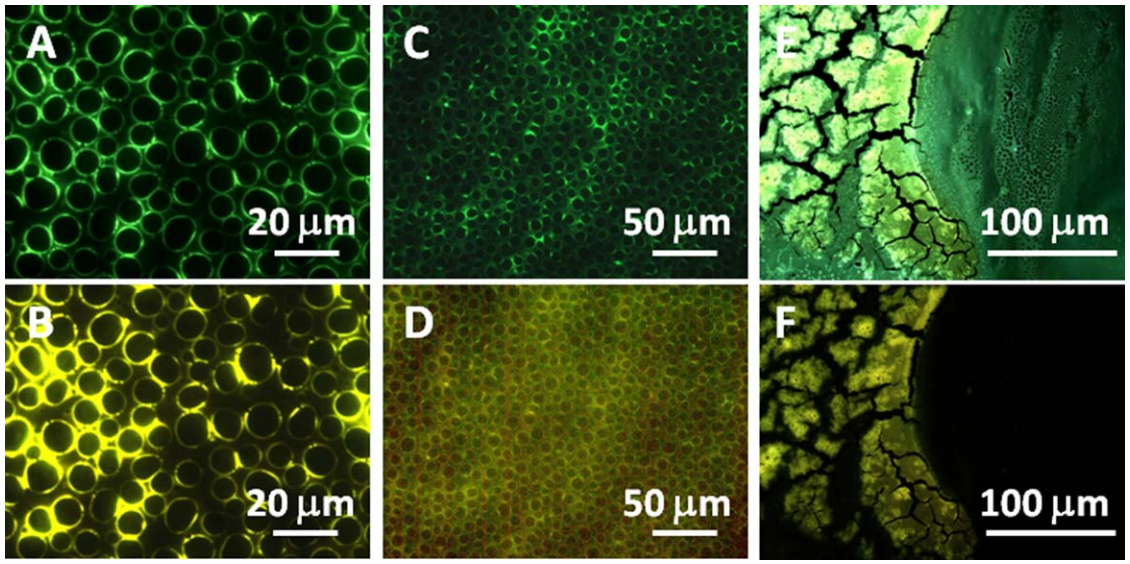

FIGURE 6 Fluorescent images of (A–D) microporous film and (E and F) its boundary of different components of *hb*–P**1** taken under UV light illumination. Excitation wavelength: (A, C, and E) 330–380 nm and (B, D and F) 450–490 nm. [Color figure can be viewed in the online issue, which is available at wileyonlinelibrary.com.]

1,2-dichloroethane, resulting in a three-dimensional negative photoresist fluorescent pattern.

To decipher the different photo-patternabilities of the hyperbranched polymers, the structure of thin film of *hb*–P**1** before and after UV irradiation for 15 min was investigated by IR and UV spectroscopies. As shown in Supporting Information Figure S10, after UV irradiation, intense new peaks associated with O–H and C=O stretching vibrations appear at 3433 and 1710 cm^{-1} in the IR spectrum, respectively, proving that the photo-oxidation reaction has taken place in the polymer. The absorption of *hb*–P**1** also shifts from 364 nm to 245 nm after

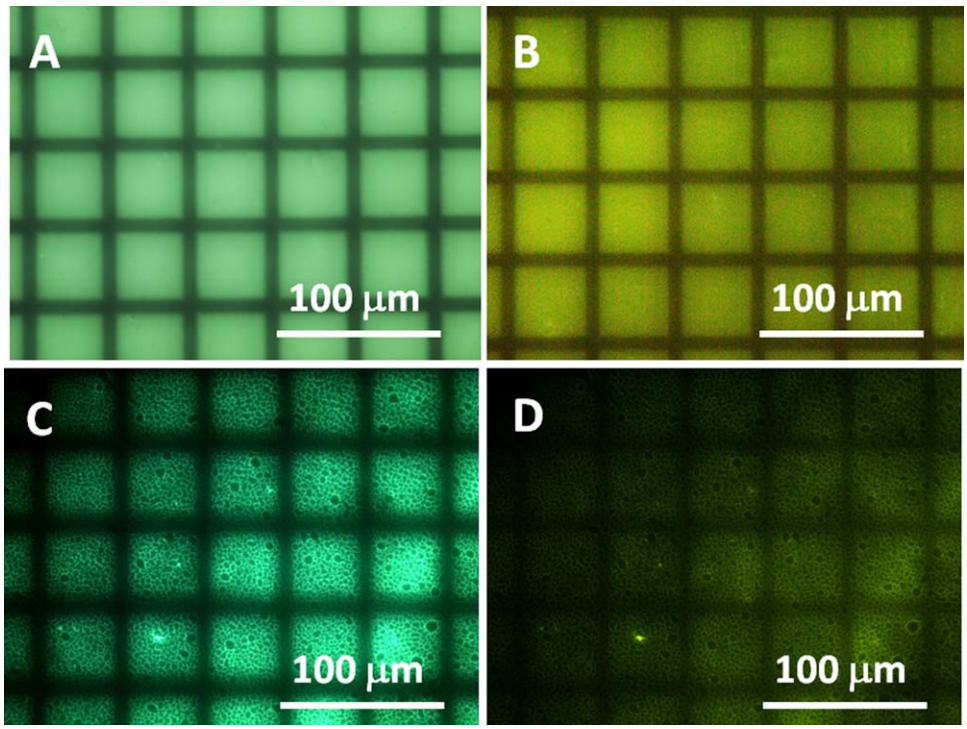

FIGURE 7 Fluorescent patterns generated by photo-oxidation of (A and B) uniform thin film and (C and D) microporous thin film of *hb*–P**1** in air at room temperature for 15 min taken under UV light illumination. Excitation wavelength: (A and C) 330–380 nm and (B and D) 460–490 nm. [Color figure can be viewed in the online issue, which is available at wileyonlinelibrary.com.]

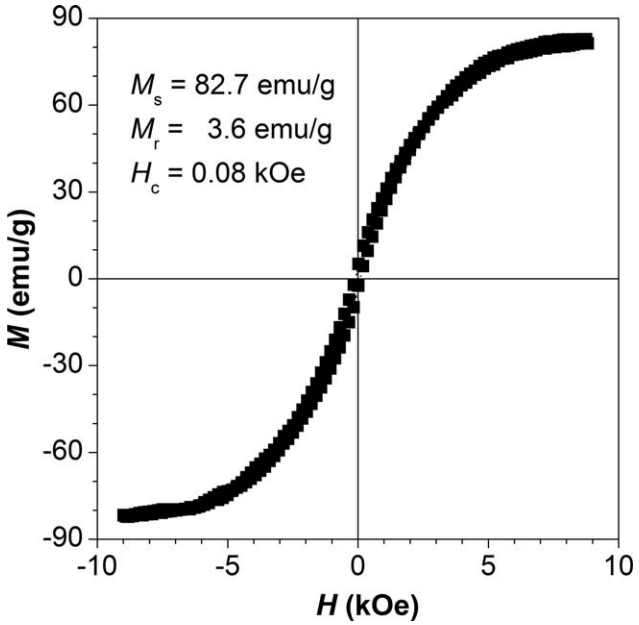

FIGURE 8 Plots of magnetization (M) versus applied magnetic field (H) at 298K for magnetoceramics MC**1**. Abbreviation: M_s = saturation magnetization in an external field of ~10 kOe, M_r = magnetic remanence at zero external field and H_c = coercivity at zero magnetization.

UV irradiation, revealing a complete loss in conjugation (Supporting Information Fig. S11). Such findings are not observed in *hb*−P**2**. Due to steric crowdedness, the TPE units in *hb*−P**1** are more twisted. Thus the central vinyl core is not well-shielded by the periphery phenyl rings, rendering it reactive. The photo-oxidation transformation of the C=C double bond to hydroxyl or carbonyl group in the presence of UV light breaks the conjugation system and hence largely quenches the fluorescence of the polymer.

The high photosensitivity of *hb*−P**1** can coupled with its self-assembly property to generate intriguing fluorescent pattern. For example, photo-oxidation of the honeycomb-patterned film in the presence of UV light through a negative copper photomask furnishes a two-dimensional fluorescent pattern with honeycomb secondary structure [Fig. 7(C,D)].

Ceramization and Magnetism

Spectroscopic analysis shows that some triple bonds of **1** remain unreacted after the polymerization and exist as end groups at the periphery of *hb*−P**1**. Acetylene triple bond is a versatile ligand and commonly used in organometallic chemistry.[31] *hb*−P**1** can thus be readily metallified through complexations with organometallic compounds as shown in Supporting Information Scheme S1.[32] $Co_2(CO)_8$ was added into the THF solution of *hb*−P**1** under nitrogen at room temperature. The solution immediately darkened in color, accompanying with CO gas evolution. The reaction mixture remained homogenous until the end of reaction and organometallic polymer *hb*−P**1**−$\{[Co(CO)_3]_2\}_x$ was obtained. Although it can dissolve during the complexation reaction, it became insoluble after purification, possibly due to the formation of supramolecular aggregates during the precipitation and drying processes. The IR spectra of *hb*−P**1** and *hb*−P**1**−$\{[Co(CO)_3]_2\}_x$ are given in Supporting Information Figure S12. The absorption band of ≡C–H stretching vibration at 3296 cm^{-1} disappears after complexation and new strong bands associated with cobalt carbonyl absorptions emerge at 2096, 2056, and 2025 cm^{-1}, suggestive of the integration of metallic species into the polymer at the molecular level.

The organometallic polymer was pyrolyzed at 1000 °C under nitrogen to form magnetic nanoparticles MC**1** in 47.8% yield. As revealed by the TEM images and ED patterns shown in Supporting Information Figure S13, the ceramics are composed of Co nanoparticles wrapped by a carboneous shell. Many diffraction spots are observed from its ED patterns, suggesting that the ceramics are crystalline in nature. XPS measurement reveals a cobalt content of 6.82% on the surface of MC**1**. The powder XRD diffractogram of MC**1** exhibits reflection peaks at 2θ angles of 44.4°, 51.8°, and 76.0° (Supporting Information Fig. S14). According to the databases of JCPDS-International Centre for Diffraction Data (ICDD), these peaks are associated with the reflections for Co metal (ICDD-data file 15–0806) (Supporting Information Fig. S15).[33] No peaks associated with the reflections of Co_xO_y have been found.

MC**1** is magnetizable and can be attracted by a bar magnet, encouraging us to investigate its magnetic properties. With an increase in the strength of external magnetic field (H), the magnetization (M) of MC**1** swiftly increases and is ultimately saturated at high field (Fig. 8). It is known that cobalt is ferromagnetic but its oxides (Co_3O_4 and CoO) are paramagnetic at room temperature.[34] MC**1** shows a high saturation value of ~83 emu/g, in agreement with its high content of ferromagnetic Co nanocrystallites. The carboneous shells may have well wrapped the cobalt nanocrystallites and prevent them from oxidation after the pyrolysis process. The coercivity (H_c) of MC**1** is found to be 0.08 kOe, suggesting that they are soft magnetic materials which may find an array of high-technology applications, especially in magnetic recording systems.

CONCLUSIONS

In this work, hyperbranched polyarylene *hb*−P**1** was synthesized in high yield with high molecular weight by homopolycyclotrimerization of A_4−type tetrayne **1** catalyzed by $TaCl_5$−$SnPh_4$ cocatalyst. The A_4 system enjoys such advantages as easier monomer preparation, simpler polymerization procedure, higher interior density of functional units and more branching sites and functional end groups in comparison with the traditional AB_n, $A_2 + B_n$ as well as A_2 strategies. *hb*−P**1** is soluble in common organic solvent such as THF, toluene, $CHCl_3$ and possesses good film-forming capability. It enjoys high thermal stability, starting to lose its weight at 525 °C under nitrogen and 461 °C in air and retaining ~60% of its weight after pyrolyzed at 800 °C. Both **1** and *hb*−P**1** are nonemissive or weakly fluorescent when molecularly dissolved in good solvent and become highly emissive

when aggregated as nanoparticle suspension in poor solvent, revealing that they are AIE or AEE-active. *hb*−P**1** functions as a sensitive fluorescent chemosensor for the detection of explosives with a novel superamplification effect. Uniform and porous fluorescent thin films are readily fabricated from *hb*−P**1** solution using the spin coating and the BF approaches, respectively. By taking advantage of the AEE feature of *hb*−P**1**, the real-time monitoring of the long-unknown BF formation process is realized. UV irradiation of the polymer films in air photo-oxidizes the polymer, generating well-resolved fluorescent photopatterns. *hb*−P**1** can be metallified by complexation of their peripheral triple bonds with cobalt carbonyl. Pyrolysis of the resulting organometallic polymer generates magnetic ceramics with high magnetic susceptibility ($M_s = 83$ emu/g) and near zero coercivity ($H_c = 0.08$ kOe), suggesting that they are good soft magnetic materials with low hysteresis loss.

ACKNOWLEDGMENTS

This work was partially supported by the National Basic Research Program of China (973 Program; 2013CB834701), the Research Grants Council of Hong Kong (604913, 604711, 602212, HKUST2/CRF/10 and N_HKUST620/11), and the University Grants Committee of HK (AoE/P-03/08). B.Z.T. is grateful for the support of the Guangdong Innovative Research Team Program (201101C0105067115).

REFERENCES AND NOTES

1 (a) D. Yan, C. Gao, H. Frey, Hyperbranched Polymers; John Wiley & Sons, Inc., Hoboken, New Jersey, USA, **2011**; (b) Y. Nakayama, *Acc. Chem. Res.* **2012**, *45*, 994−1004; (c) H. Jin, W. Huang, X. Zhu, Y. Zhou, D. Yan, *Chem. Soc. Rev.* **2012**, *41*, 5986–5997; (d) D. S. Thompson, L. J. Markoski, J. S. Moore, I. Sendijarevic, A. Lee, A. J. McHugh, *Macromolecules* **2000**, *33*, 6412−6415; (e) H. T. Chang, J. M. J. Fréchet, *J. Am. Chem. Soc.* **1999**, *121*, 2313−2314; (f) B. Voit, *J. Polym. Sci. Polym. Chem.* **2000**, *38*, 2505−2525; (g) L. Zhi, J. Wu, J. Li, M. Stepputat, U. Kolb, K. Müllen, *Adv. Mater.* **2005**, *17*, 1492−1496.

2 (a) Z. Xue, A. D. Finke, J. S. Moore, *Macromolecules* **2010**, *43*, 9277−9282; (b) Z. Dong, Z. Ye, *Polym. Chem.* **2012**, *3*, 286−301; (c) R. Hu, J. W. Y. Lam, B. Z. Tang, *Macromol. Chem. Phys.* **2013**, *214*, 175−187; (d) J. P. Majoral, A. M. Caminade, *Chem. Rev.* **1999**, *99*, 845−880; (e) A. W. Bosman, H. M. Janssen, E. W. Meijer, *Chem. Rev.* **1999**, *99*, 1665−1688; (f) R. Van Heerbeek, P. J. C. Kamer, P. W. N. M. Van Leeuwen, J. N. H. Reek, *Chem. Rev.* **2002**, *102*, 3717−3756; (g) S. M. Grayson, J. M. J. Fréchet, *Chem. Rev.* **2001**, *101*, 3819−3867; (h) F. Zeng, S. C. Zimmerman, *Chem. Rev.* **1997**, *97*, 1681–1712.

3 (a) T. V. Rao, H. Yamashita, Y. Uchimaru, J. Sugiyama, K. Takeuchi, *Polymer*, **2005**, *46*, 9736−9741; (b) G. Kwak, A. Takagi, M. Fujiki, T. Masuda, *Chem. Mater.* **2004**, *16*, 781−785; (c) W. Wu, S. Ye, L. Huang, L. Xiao, Y. Fu, Q. Huang, G. Yu, Y. Liu, J. Qin, Q. Li, Z. Li, *J. Mater. Chem.* **2012**, *22*, 6374−6382.

4 (a) J. M. J. Fréchet, M. Henmi, I. Gitsov, S. Aoshima, M. R. Leduc, R. B. Grubbs, *Science*, **1995**, *269*, 1080−1083; (b) H. C. Yang, S. Y. Lin, H. C. Yang, C. L. Lin, L. Tsai, S. L. Huang, I. W. P. Chen, C. H. Chen, B. Y. Jin, T. Y. Luh, *Angew. Chem. Int. Ed. Engl.* **2006**, *45*, 726−730.

5 M. Häußler, B. Z. Tang, *Adv. Polym. Sci.* **2007**, *209*, 1−58.

6 (a) R. Zheng, J. W. Y. Lam, H. Peng, M. Häußler, B. Z. Tang, *Polym. Mater. Sci. Eng.* **2003**, *88*, 365; (b) M. Häussler, J. Z. Liu, R. Zheng, B. Z. Tang, *Macromolecules* **2007**, *40*, 1914−1925.

7 M. G. McKee, S. Unal, G. L. Wilkes, T. E. Long, *Prog. Polym. Sci.* **2005**, *30*, 507−539.

8 H. R. Kricheldorf, *Pure Appl. Chem.* **1998**, *70*, 1235−1238.

9 (a) J. D. Luo, Z. L. Xie, J. W. Y. Lam, L. Cheng, H. Y. Chen, C. F. Qiu, H. S. Kwok, X. W. Zhan, Y. Q. Liu, D. B. Zhu, B. Z. Tang, *Chem. Commun.* **2001**, 1740−1741; (b) Y. Hong, J. W. Y. Lam, B. Z. Tang, *Chem. Soc. Rev.* **2011**, *40*, 5361−5388; (c) J. Huang, N. Sun, Y. Q. Dong, R. L. Tang, P. Lu, P. Cai, Q. Q. Li, D. G. Ma, J. G. Qin, Z. Li, *Adv. Funct. Mater.* **2013**, *23*, 2329−2337; (d) J. Huang, X. Yang, X. J. Li, P. Y. Chen, R. L. Tang, F. Li, P. Lu, Y. G. Ma, L. Wang, J. G. Qin, Q. Q. Li, Z. Li, *Chem. Commun.* **2012**, *48*, 9586−9588; (e) J. Huang, X. Yang, J. Y. Wang, C. Zhong, L. Wang, J. G. Qin, Z. Li, *J. Mater. Chem.* **2012**, *22*, 2478−2484.

10 R. Hu, J. W. Y. Lam, J. Liu, H. H. Y. Sung, I. D. Williams, Z. Yue, K. S. Wong, M. M. F. Yuen, B. Z. Tang, *Polym. Chem.* **2012**, *3*, 1481−1489.

11 J. Wang, J. Mei, E. Zhao, Z. Song, A. Qin, J. Z. Sun, B. Z. Tang, *Macromolecules* **2012**, *45*, 7692−7703.

12 J. W. Y. Lam, J. Chen, C. C. W. Law, H. Peng, Z. Xie, K. K. L. Cheuk, H. S. Kwork, B. Z. Tang, *Macromol. Symp.* **2003**, *196*, 289−300.

13 Z. Chi, X. Zhang, B. Xu, X. Zhou, C. Ma, Y. Zhang, S. Liu, J. Xu, *Chem. Soc. Rev.* **2012**, *41*, 3878−3896.

14 N. Zhao, Z. Yang, J. W. Y. Lam, H. H. Y. Sung, N. Xie, S. Chen, H. Su, M. Gao, I. D. Williams, K. S. Wong, B. Z. Tang, *Chem. Commun.* **2012**, *48*, 8637−8639.

15 (a) S. W. Thomas, G. D. Joly, T. M. Swager, *Chem. Rev.* **2007**, *107*, 1339−1386; (b) U. H. F. Bunz, *Chem. Rev.* **2000**, *100*, 1605−1644; (c) S. J. Toal, W. C. Trogler, *J. Mater. Chem.*, **2006**, *16*, 2871−2883; (d) H. Nie, Y. Zhao, M. Zhang, Y. Ma, M. Baumgarten, K. Müllen, *Chem. Commun.* **2011**, *47*, 1234−1236.

16 J. B. Birks, Photophysics of Aromatic Molecules; Wiley: London, **1970**.

17 (a) Y. Che, D. E. Gross, H. Huang, D. Yang, X. Yang, E. Discekici, Z. Xue, H. Zhao, J. S. Moore, L. Zang, *J. Am. Chem. Soc.* **2012**, *134*, 4978−4982; (b) R. Hu, J. L. Maldonado, M. Rodriguez, C. Deng, C. K. W. Jim, J. W. Y. Lam, M. M. F. Yuen, G. R. Ortiz, B. Z. Tang, *J. Mater. Chem.* **2012**, *22*, 232−240; (c) J. Liu, Y. Zhong, P. Lu, Y. Hong, J. W. Y. Lam, M. Faisal, Y. Yu, K. S. Wong, B. Z. Tang, *Polym. Chem.* **2010**, *1*, 426−429.

18 J. C. Sanchez, A. G. Dipasquale, A. L. Rheingold, W. C. Trogler, *Chem. Mater.* **2007**, *19*, 6459−6470.

19 (a) P. Lu, J. W. Y. Lam, J. Liu, C. K. W. Jim, W. Yuan, C. Y. K. Chan, N. Xie, Q. Hu, K. K. L. Cheuk, B. Z. Tang, *Macromolecules* **2011**, *44*, 5977−5986; (b) M. Gao, J. W. Y. Lam, J. Li, C. Y. K. Chan, Y. Chen, N. Zhao, T. Han, B. Z. Tang, *Polym. Chem.* **2013**, *4*, 1372−1380.

20 (a) T. Nakamura, N. Tsutsumi, *J. Appl. Phys.* **2005**, *97*, 054505; (b) M. Suwa, H. Niwa, M. Tomikawa, *J. Photopolym. Sci. Technol.* **2006**, *19*, 275−276; (c) J. L. Regolini, D. Benoit, P. Morin, *Microelectron Reliab.* **2007**, *47*, 739−742.

21 R. Hu, J. W. Y. Lam, Y. Yu, H. H. Y. Sung, I. D. Williams, M. M. F. Yuen, B. Z. Tang, *Polym. Chem.* **2013**, *4*, 95−105.

22 C. K. W. Jim, J. W. Y. Lam, A. Qin, Z. Zhao, J. Liu, Y. Hong, B. Z. Tang, *Macromol. Rapid Commun.* **2012**, *33*, 568−572.

23 (a) L. Heng, J. Zhai, Y. Zhao, J. Xu, X. Sheng, L. Jiang, *ChemPhysChem*, **2006**, *7*, 2520−2525; (b) U. Stalmach, B. de

Boer, C. Videlot, P. F. van Hutten, G. Hadziioannou, *J. Am. Chem. Soc.*, **2000**, *122*, 5464−5472; (c) M. E. Davis, *Nature* **2002**, *417*, 813−821; (d) M. Campbell, D. N. Sharp, M. T. Harrison, R. G. Denning, A. J. Turberfield, *Nature* **2000**, *404*, 53−56; (e) D. Beattie, K. H. Wong, C. Williams, L. A. Poole-Warren, T. P. Davis, C. Barner-Kowollik, M. H. Stenzel, *Biomacromolecules* **2006**, *7*, 1072−1082.

24 (a) Y. Yu, Y. Ma, *Soft Matter* **2011**, *7*, 884−886; (b) B. de Boer, U. Stalmach, H. Nijland, G. Hadziioannou, *Adv. Mater.* **2000**, *12*, 1581−1583.

25 G. Widawski, B. Rawiso, B. François, *Nature* **1994**, *369*, 387−389.

26 (a) E. Ferrari, P. Fabbri, F. Pilati, *Langmuir* **2011**, *27*, 1874−1881; (b) C. Y. Ma, Y. W. Zhong, J. Li, C. K. Chen, J. L. Gong, S. Y. Xie, L. Li, Z. Ma, *Chem. Mater.* **2010**, *22*, 2367−2374.

27 K. C. Stylianou, R. Heck, S. Y. Chong, J. Bacsa, J. T. A. Jones, Y. Z. Khimyak, D. Bradshaw, M. J. Rosseinsky, *J. Am. Chem. Soc.* **2010**, *132*, 4119−4130.

28 A. Böker, Y. Lin, K. Chiapperini, R. Horowitz, M. Thompson, V. Carreon, T. Xu, C. Abetz, H. Skaff, A. D. Dinsmore, T. Emrick, T. P. Russell, *Nat. Mater.* **2004**, *3*, 302−306.

29 S. A. Jenekhe, X. L. Chen, *Science* **1999**, *283*, 372−375.

30 C. Liu, C. Gao, D. Yan, *Angew. Chem. Int. Ed. Engl.* **2007**, *46*, 4128−4131.

31 (a) G. R. Newkome, E. F. He, C. N. Moorefield, *Chem. Rev.* **1999**, *99*, 1689−1746; (b) W. Y. Chan, A. Berenbaum, S. B. Clendenning, A. J. Lough, I. Manners, *Organometallics* **2003**, *22*, 3796−3808.

32 (a) A. Berenbaum, M. Ginzburg-Margau, N. Coombs, A. J. lough, A. Safa-Sefat, J. E. Greedan, G. A. Ozin, I. Manners, *Adv. Mater.* **2003**, *15*, 51−55; (b) R. J. P. Corriu, N. Devylder, C. Guerin, B. Henner, A. Jean, *J. Organomet. Chem.* **1996**, *509*, 249−257.

33 M. Häuβler, J. W. Y. Lam, R. H. Zheng, H. C. Dong, H. Tong, B. Z. Tang, *J. Inorg. Organomet. Polym. Mater.* **2006**, *15*, 519−526.

34 R. C. O'Handley, Modern Magnetic Materials: Principles and Applications; Wiley: New York, **2000**.